

In-Flight Engine Diagnostics and Prognostics Using A Stochastic-Neuro-Fuzzy Inference System

Dan M. Ghiocel & Joshua Altmann
STI Technologies, Rochester, New York, USA

Keywords: reliability, stochastic fields, turbine, series expansion, response surface, random

ABSTRACT: One key aspect when developing a robust health management system for turbines is the development of accurate and robust fault classifiers. The paper illustrates the application of a hybrid *Stochastic-Neuro-Fuzzy-Inference System* to fault diagnostics and prognostics for turbine performance. The random fluctuations of turbine performance parameters in different varying operating conditions are modeled using a multivariate stochastic model. At any time, the fault risk condition is approached as a conditional reliability problem based on the measurement of parameter deviations from the normal operating condition. The paper illustrates the application of the proposed system to a typical aircraft turbofan engine for in-flight engine performance diagnostic and prognostic.

1 TURBINE THROUGH FLOW ANALYSIS MODELING

Figure 1 shows a sketch of a typical turbofan engine including the performance parameters considered herein for fault diagnostic and prognostic. Figures 2 and 3 show pressure variations as a function of the high-pressure shaft speed stationary conditions versus highly transient operating conditions, respectively. It is obvious from these figures that although for slowly varying conditions the pressure closely follows a nonlinear relationship with shaft speed, for highly transient operating conditions the pressure deviates from this nonlinear path due to highly transient conditions and significant changes in the inlet conditions, namely inlet pressure, temperature and mass flow. This means using deviations from a fitted polynomial regression line for diagnostics, as commonly used in engine health monitoring application based on ground-test data, is not suited to in-flight conditions. In fact the large stochastic variability projected on the pressure-speed plane in Figure 3 is only apparent. This large variability is mostly due the transient variations induced by the pilot maneuvers. A key aspect for getting realistic predictions for in-flight operating conditions is to separate the *true statistical variabilities* (random part) from the *functional variabilities* introduced by engine transient behavior. For fast transient conditions the functional dependence between turbine performance parameters becomes complex and highly nonlinear. If these transient functional dependencies between multiple parameters are ignored then the statistical variability is overestimated and the computed fault risks are unreliable, being overestimated as shown in Figure 3.

As physics-based, analytical GPA models only cater for quasi-stationary engine operation, an alternative scheme capable of including the highly transient in-flight conditions has been developed. This lead to the formation of a stochastic diagnostic-prognostic model based on parameter statistical deviations from an adaptive network-based fuzzy inference system GPA model. This model was developed by calibrating the analytical GPA model, and tuning its stochastic input-output using an adaptive networked-based fuzzy inference system model (ANFIS) based on training from typical transient operating data for a given turbine type. A hybrid neural net was then used to finely tune the fuzzy inference models using both least-square and back-propagation algorithms. The multiple statistical deviations of the measured engine parameters from the ANFIS model outputs are modeled using a multidimensional stochastic vector process with correlated components. A twenty and, respectively, a twenty-four stochastic state vector dimension was used to define the reliability function (g-function) for the engine fault diagnostic (twice the physical parameter number, ten physical parameters for the transient model and respectively twelve physical parameters for the quasi-static model).

A key aspect while developing the engine GPA model was how to handle multiple-cascaded engine faults when a downstream engine fault can shadowed by an upstream engine fault. To handle cascaded faults, compartmentalized GPA models were developed for each engine compartment as indicated in Figure 4. Using compartmentalized GPA models cascaded multiple turbine engine faults can be accurately diagnosed. No fault interactions were included in the GPA model.

There are two major advantages that are provided by including a compartmentalized GPA model to complement the overall GPA model: (i) increased resolution of parameters is available, as uncertainty introduced by other compartments is eliminated and (ii) ability to discriminate between the presence of single and multiple compartment faults in engine.

An overall GPA model can lead to difficulties in diagnosing the cause and mapping the progression of faults if two or more compartments are operating out of specification as shown in Figure 4. The main drawback of the compartmentalized GPA model is that one loses the multidimensional parameter space, i.e. interaction between engine parameters that is available in the overall GPA model. At most two parameters, the pressure and temperature, are available in the transient ANFIS GPA model. Both methods should be incorporated to make use of the synergies that can be attained from these models. The in-flight performance data based on measurements of normal operating conditions were used to provide the baseline for generating the GPA models.

Figures 5 and 6 illustrate the importance of using a multidimensional ANFIS GPA model to determine with a high degree of accuracy the parameter statistical deviations from normal operating conditions. The effects of high-pressure turbine efficiency drop on the deviations are shown on the parameters P_5 , T_6 and P_6 . Figure 5, which is based temperature and pressure deviations from a fifth-order polynomial fitting of engine parameters against the high pressure rotor speed (parameters are one-dimensional functions), is inadequate for fault detection due to the apparent large degree of uncertainty in measurements. In comparison, the ANFIS GPA models shrinks that uncertainty to a level that small changes in operating efficiency or capacity from normal status can be detected (parameters are fifth-dimensional functions). This improvement in stochastic fault resolution detection is a key factor for an accurate risk-based fault diagnostic and prognostic of the engine condition.

The GPA model was used to simulate engine faults with the corresponding parameter input-output relationships mapped onto the ANFIS model. The fault statistical parameter deviations from the ANFIS output were idealized by a non-zero stochastic state vector process with correlated components. As can be noticed from Figure 7 the marginal probability density functions (MPDF) of these deviations can be non-Gaussian. In addition some of the statistical parameter deviations can be highly correlated as illustrated by the time histories plotted in Figure 8. The pair correlation functions of the deviation histories plotted in Figure 8 are shown in Figure 9. These correlation functions plotted for normal conditions and fault conditions are compared for two adjacent compartment pressure-pressure pair and for a pressure-temperature pair. Figure 9 indicates that fault conditions may affect significantly the correlation length (Figure 9a) of the process and also its instantaneous correlation (Figure 9b).

2 RELIABILITY-BASED DIAGNOSTICS AND PROGNOSTICS

As discussed in the previous section, engine parameter measured on-line include pressures, temperatures and fuel flows in different compartments of an engine. A pictorial overview of the proposed probabilistic fault diagnostic/prognostic procedure is illustrated in Figure 10 (a two-dimensional parameter space representation was used for visualization purposes). As shown in Figure 10 for the usage path 3, at a given time the engine condition can be diagnosed by evaluating all the risks of potential engine faults. Figure 11 shows the engine performance degradation from usage point P1 to usage point P2. To compute the fault reliability index, first the performance safety margin, called also performance function needs to be defined. This performance safety margin in the engine parameter space was defined by the distance between the measurement variability ellipsoid (cluster) and the fault variability ellipsoid (cluster) as shown in Figure 11. Figure 11 shows that this distance can be defined in two ways: (i) a linear distance

between the two multidimensional ellipsoids, as safety margin of Type A, (ii) or as arc-length defined by the curvilinear usage trajectory, as safety margin of Type B.

To diagnose the engine fault risks and also to prognostic them for in-flight conditions the First-Order Reliability Method (FORM) and Monte Carlo simulation (MCS) were employed. Using these two probabilistic approaches, FORM and MCS, the fault reliability indices for any point on the predicted trajectory from measured location and to different point locations within the fault basin of attraction can be computed. The reliability index computed for current measurement location is used for fault diagnostics. Reliability indices computed for locations on the future projected usage trajectory, from a predicted location to the fault location, are used for prognostics. The associated fault diagnostic and prognostic probabilities, P_f , in the multidimensional parameter space are determined based on the computed reliability index, β using the FORM approximation:

$$P_f \approx \Phi(-\beta) \quad (3)$$

where $\Phi(\cdot)$ is the standard Gaussian cumulative distribution function. To determine the usage rate in probabilistic terms (measurement location speed on the trajectory) the reliability index gradients required. Specifically, two reliability index sensitivity measures are introduced: (i) a cumulative and (ii) an evolutionary sensitivity index. The cumulative reliability sensitivity index (CRSI) is defined by the “global” non-dimensional variation of the FORM reliability index, β (the relation between “failure probability”, here read fault diagnostic probability, and reliability index is discussed on the next page) from initial state, at 0, to the final state, at t (over the interval [0, t]):

$$C_{0,t} = -\frac{\beta_t - \beta_0}{\beta_0} = -\frac{\Delta\beta_{0,t}}{\beta_0} \quad (4)$$

The evolutionary reliability sensitivity index (ERSI) is defined by the “local” non-dimensional variation of the reliability index, from an intermediary state, at time t_i , to another intermediary state, at time t_i+1 (over $[t_i, t_i+1]$):

$$E_{t_i,t_i+1} = -\frac{\beta_{t_i+1} - \beta_{t_i}}{\beta_{t_i}} = -\frac{\Delta\beta_{t_i,t_i+1}}{\beta_{t_i}} \quad (5)$$

These two reliability sensitivity indices indicate in percentage the changes engine reliability. A zero value indicates no safety (performance) degradation, while a positive value indicates a safety (performance) degradation and a negative value indicates safety improvement. Robustness indices (RI) can be defined as inverse of sensitivity indices (SI). For the engine performance degradation problem the “red” alarms can be set; for example, for fault diagnostic a lower bound of reliability index of 3.70 (equivalent to FORM fault probability of 0.0001) can be accepted; or for fault prognostic a CRSI of 0.5 or equivalently CRR of 2.0, and a ERSI of 0.2, or equivalently a ERRI of 5.0 can be set as alarm levels.

3 ILLUSTRATIVE EXAMPLE

The probability distributions of faults are defined for a given severity level in the engine efficiency loss. They are determined experimentally and/or numerically by “seeded” faults using test results and GPA-model simulation results as shown in Figure 12. In this illustrative example, for the sake of simplicity, the faults were defined by point locations rather than basins of attraction. The probabilistic fault diagnostic-prognostic procedure is illustrated in Figure 13. For reliability calculations a safety margin of type A was used. As discussed in the previous section, due to the engine usage the measured parameters depart from the origin (zero usage). The measured parameter set begins to shift as the performance degradation occurs. After a number of engine flights, the anomaly detection level is reached, and thus an anomaly warning becomes active. At this point, the fault diagnostic becomes of interest.

Consider now, that after another number of flights the measured parameter variability ellipsoid moves to the point location P1. At this point, the fault diagnostic reliability index decreases for Fault 3 or a Fault 4. However, after a continued operation the measured data moves toward point P2, which will be classified with a highest degree of confidence as Fault 4. These faults are Faults 1 is a fan efficiency

degradation, Fault 3 is a high-pressure compressor efficiency degradation, and Fault 4 is a high-pressure turbine efficiency degradation manifest in the parameter space. The safety margin becomes gradually smaller from point P1 to point P2, as engine performance degrades. Figure 14 shows how the engine (reliability) performance index, β , varies for the two different measured usage conditions, P1 and P2, with respect to the Faults 1, 3 and 4

Figure 15 illustrates the computed values of CRSI for usage locations P1 and P2, and ERSI for interval P1-P2. The negative values of CRSI and ERSI indicate a departure from a specific fault, while the positive values indicate a movement toward a specific fault. The CRSI and ERSI evolutions show that performance degradation was initially in the directions of both Fault 3 and Fault 4 for the Origin-P1 usage path, but then for P1-P2 usage path mostly in the direction of Fault 4, departing from the other faults. Different values of these reliability indices can be set for requesting essential and preventive maintenance activities as suggested in Figures 14 and 15. The absolute reliability index values are the basis of the risk-based fault diagnostic, while the sensitivity reliability indices are the basis for risk-based prognostics (an additional key aspect for a realistic prognostic is to anticipate any significant change in future flight conditions). At any instant time, the projected remaining life of the engine can be assessed for a given fault severity using the computed reliability loss between two consecutive measurement times. If there are 1000 flight hours for an usage evolution from P1 to P2 that corresponds to a reliability index decrease of 4.25, then assuming a minimum accepted reliability index of 3.70, the computed remaining engine safe life is 130 flight hours.

Figures 16 and 17 illustrate the variation of reliability index for a fan fault expressed by a 3% drop in engine efficiency. Figure 16 shows the variation of reliability index for all potential faults considered, while Figure 17 shows the variation of the reliability sensitivity index for all potential faults. These results were computed using the quasistatic engine model.

5 CONCLUDING REMARKS

A *Stochastic-Neuro-Fuzzy-Inference System* was proposed as a basis of a future robust *Prognostic EHMS*. The proposed predictive system is a combination of advanced stochastic modeling with an adaptive network-based fuzzy modeling for engine performance data. The system is capable of extracting and using more refined statistical information for fault classification and prognostic, than a typical EHMS based on a pure neural-net fuzzy logic-inference approach.

As shown in the paper, there is a significant useful information in the correlation structure of multidimensional measured parameter deviations that are incorporated in much greater detail in the proposed hybrid stochastic-fuzzy approach than in a standard AI fuzzy-logic approach based on a fuzzy approximation of statistical data. In addition to traditional AI approaches for EHMS, the proposed hybrid stochastic-fuzzy system can quantify the engine fault risks at any given time and project their evolution in the future for engine fault prognostics.

6 REFERENCES

- Altmann J., Mathew J. 1999. Automated DWPA Feature Extraction of Fault Information from Low Speed Rolling-Element Bearings”, Asia-Pacific Vibration Conference, Singapore
- Ghiocel, D.M. and Gasparini, D.A., 1995. Evaluation of Nonlinear Stochastic Response Using Continuation and Simulation Techniques, Proceedings of ICASP 7, Vol. 2, Paris, France, July 10-13
- Ghiocel, D.M., 2000. Advanced Stochastic Classifiers for Jet Engine Performance and Vibration. 55thMFPT Conference, Virginia Beach, NC, May 4-6

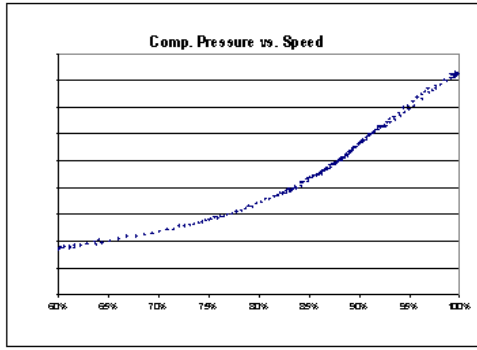


Fig. 2. P3 vs. ω_{gg} for ground tests

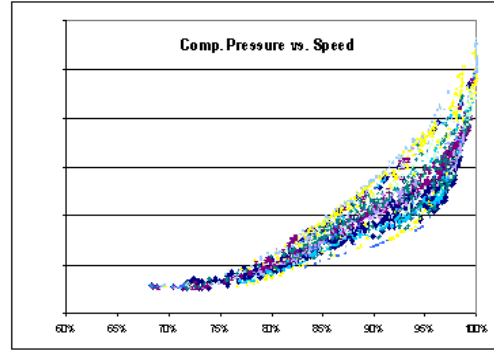


Fig. 3. P3 vs. ω_{gg} for in-flight conditions

Transient Engine Models:

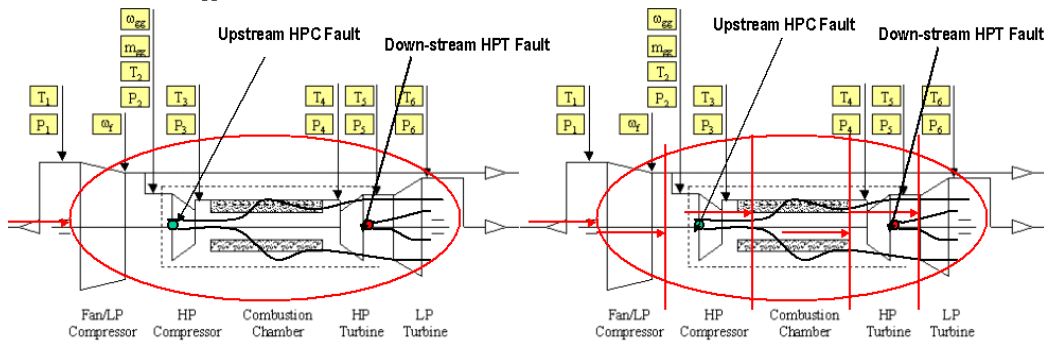
$$P_n, T_n = \text{fn}(P_1, T_1, \dot{m}_{gg}, \omega_f, \omega_{gg})$$

$$P_n, T_n = \text{fn}(P_{n-1}, T_{n-1}, \dot{m}_{gg}, \omega_f, \omega_{gg})$$

Quasi-Stationary Engine Models:

$$P_n, T_n, \dot{m}_{gg}, \omega_f = \text{fn}(P_1, T_1, \omega_{gg})$$

$$P_n, T_n = \text{fn}(P_{n-1}, T_{n-1}, \omega_{gg})$$



a) Overall GPA Model

b) Compartmentalized GPA Models

Fig. 4. Schematic of the Overall and Compartmentalized GPA Models

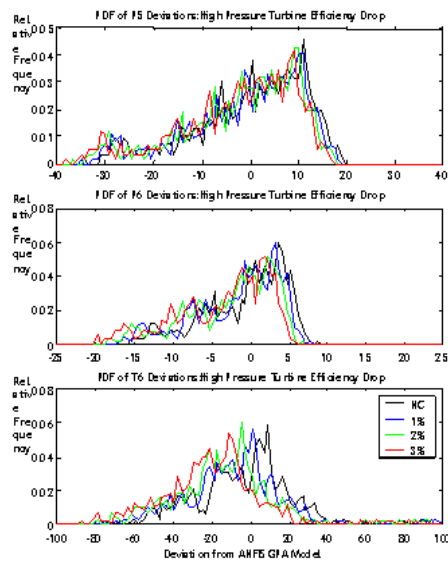


Fig. 5. PDF of deviations for the polynomial GPA model for in-flight conditions

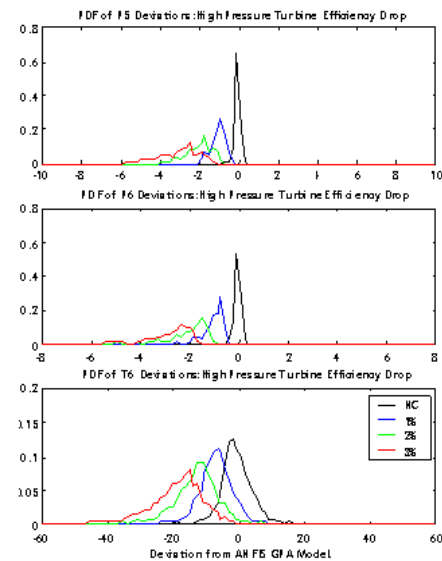


Fig. 6. PDF of deviations for the ANFIS GPA model for in-flight conditions

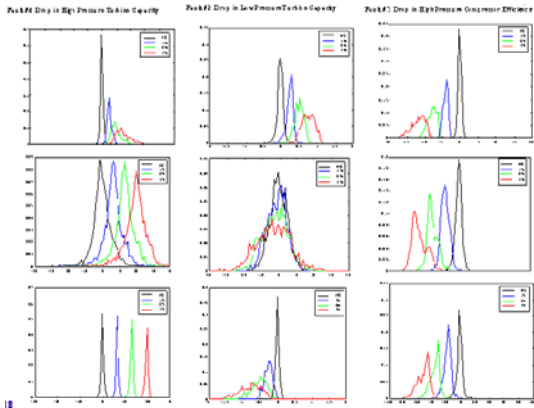


Fig. 7. MPDFs of parameter deviations

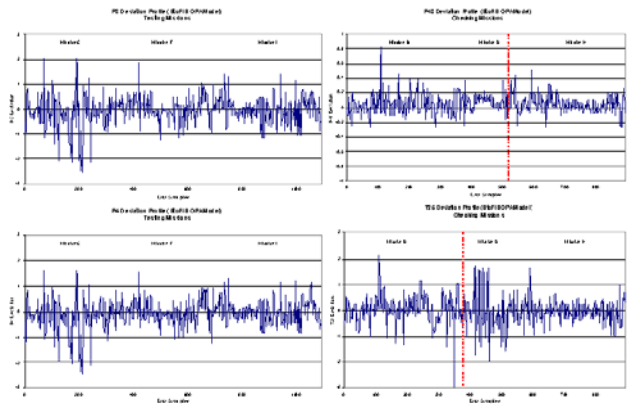
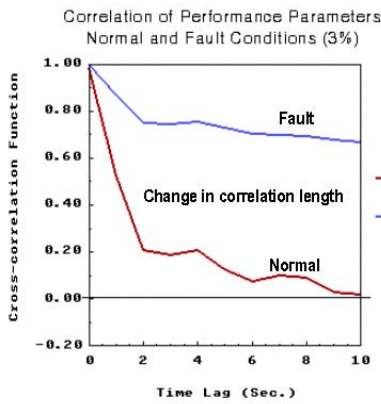
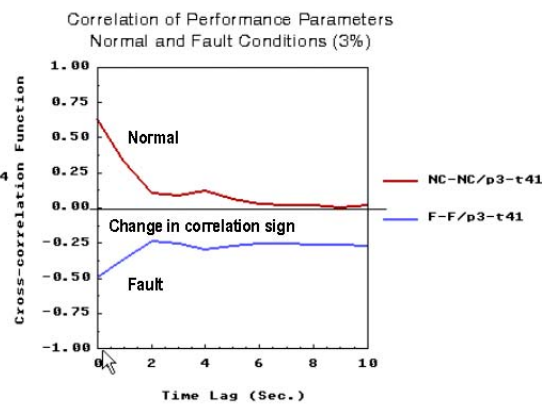


Fig. 8. Adjacent pressures and pressure-temperature pair histories



a) P3-P4 cross-correlation function



b) T25-P48 cross-correlation function

Fig. 9. Pair correlation functions for normal conditions (NC-NC) and fault conditions (F-F)

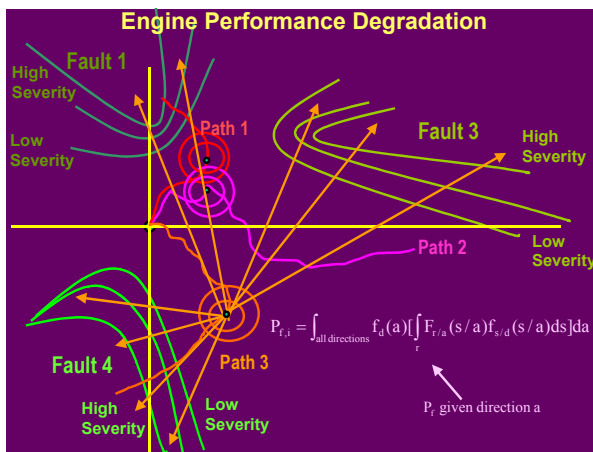


Fig. 10. Engine Performance Degradation

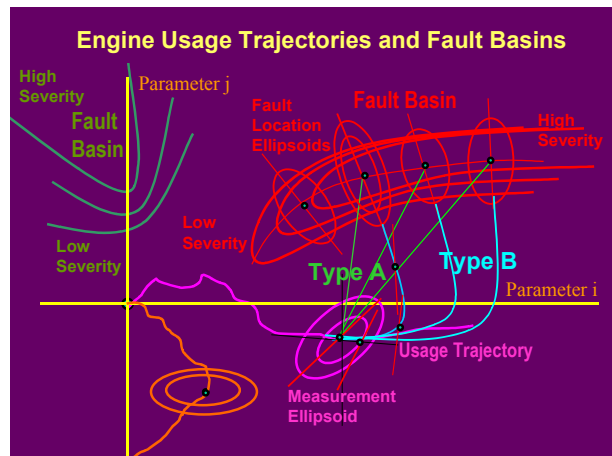


Fig. 11. Performance Degradation Trajectories

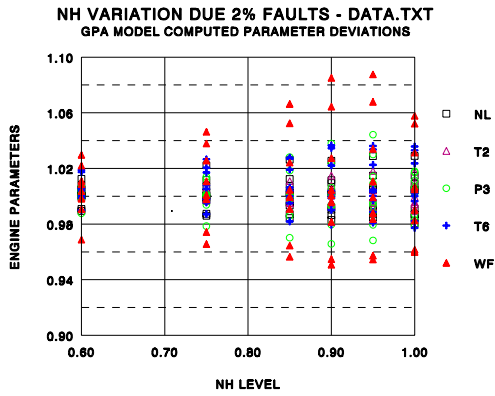


Fig.12. Fault Patterns for 2% Efficiency Drop

Diagnostics:
Reliability Index

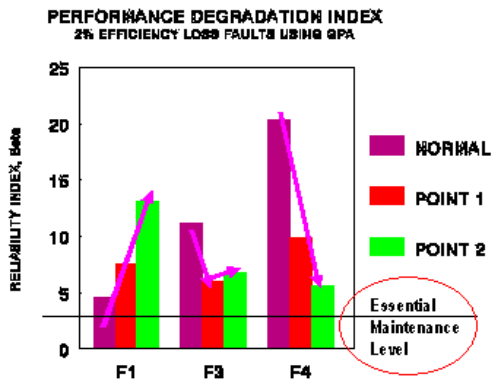


Fig. 14. Reliability Index Evolution

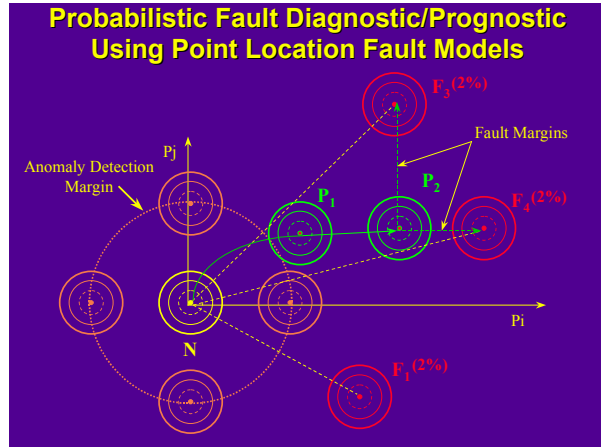


Fig.13. Probabilistic Fault Diagnostic/Prognostic

Prognostics:
Reliability Sensitivity Index

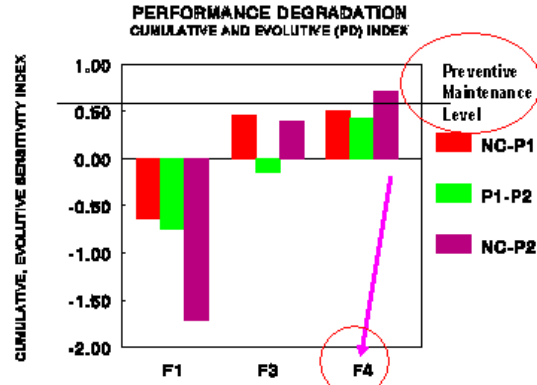


Fig. 15. ERSI and CRSI Evolution

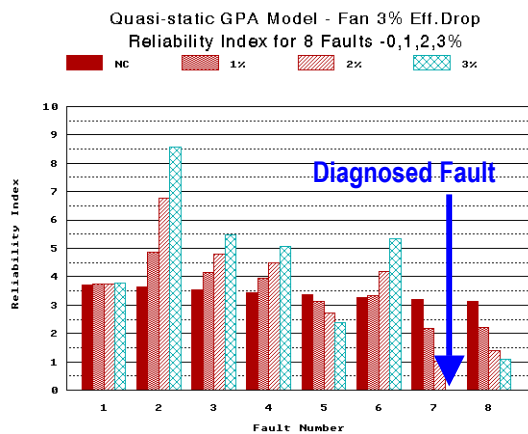


Fig. 16. Computed Reliability Index

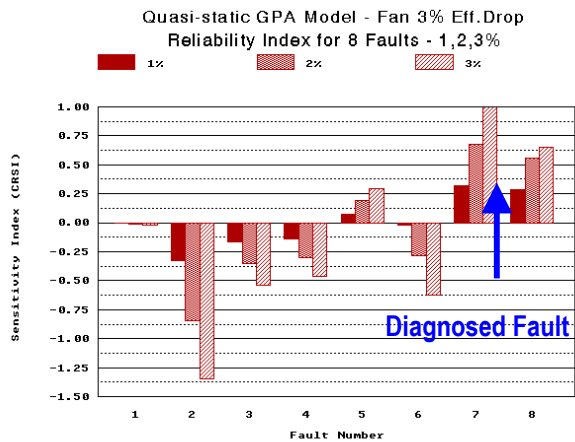


Fig. 17. Reliability Sensitivity Index